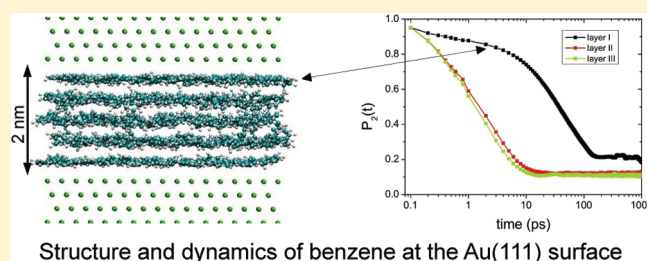


Properties of Benzene Confined between Two Au(111) Surfaces Using a Combined Density Functional Theory and Classical Molecular Dynamics Approach

Karen Johnston^{*,†} and Vagelis Harmandaris^{*,‡}[†]Max-Planck Institute for Polymer Research, P.O. Box 3148, Mainz 55021, Germany, and[‡]Department of Applied Mathematics, University of Crete and IACM-FORTH, GR-71409 Heraklion, Crete, Greece

ABSTRACT: The study of the effect of confinement on the structural and dynamical properties of fluids is an intense research field. Here we present results about benzene confined between gold Au(111) surfaces, from a hierarchical dualscale simulation methodology. The adsorption energies and structures of a single benzene molecule on the Au(111) surface were calculated using density functional theory with van der Waals forces. The results were used to develop an accurate classical all-atom force field for the interaction between benzene and the Au(111) surface, capable of predicting various adsorption sites and molecule orientations. Molecular dynamics simulations were used to study benzene films, of various thicknesses, between two parallel gold surfaces. Density, conformations, and dynamics of confined benzene are studied and compared to bulk properties.



Structure and dynamics of benzene at the Au(111) surface

Molecular dynamics simulations were used to study benzene films, of various thicknesses, between two parallel gold surfaces. Density, conformations, and dynamics of confined benzene are studied and compared to bulk properties.

1. INTRODUCTION

The study of confined molecular fluids is a very active research area because of their importance in a variety of scientific problems and technological processes such as nanolithography, catalysis, lubrication, and hybrid fluid/solid composite materials. In this field the study of the fluid properties at the molecular scale is very important since the structural and dynamical behavior of soft matter is changed radically under confinement. For this reason there are many experimental studies of liquids in nanopores, with benzene liquid and silica or graphite nanopores being among the most commonly studied materials.^{1–6}

Among the properties studied, the phase transition behavior of confined benzene has been extensively examined. It has been found that phase transition temperatures and pressures are often shifted from the bulk values and new structures can appear due to surface forces.⁷ For example, the phase transition behavior of benzene in silicate nanopores has been studied using various experimental techniques.¹ The melting temperature decreased with decreasing pore size, although only partial crystallization was observed which indicates that a transition to a glassy state occurred. Watanabe et al.² also studied benzene in graphitic nanopores and observed that the melting temperature is higher for the confined system than for the bulk. Furthermore, the structure of nanoconfined benzene has been studied through neutron diffraction experiments.³ It has been shown that for large pores the static structure factor of benzene is very similar to the bulk one, whereas systematic differences were found on decreasing the size of the pores.

The dynamics of nanoconfined molecular liquids has also been studied through experimental techniques. Most of these works use ultrafast spectroscopy to study the dynamics of confined liquids.

Fourkas and collaborators study the dynamics of confined benzene in nanoporous sol–gel glass monoliths with a range of average pore sizes.^{5,6} They found that the orientational dynamics of benzene is strongly influenced by the confinement and related this to the strong ordering of benzene molecules in the nanopores. The incoherent intermediate scattering function of confined toluene has also been calculated from elastic neutron scattering experiments³ and a more heterogeneous dynamics of the confined toluene, compared to the bulk, was observed.

The experimental findings, such as the case of silica nanopores mentioned above, highlight the dependence of the properties on the interaction with the interface and to really understand the interfacial chemistry it is necessary to use simulations. To be specific, atomistic molecular simulations offer a valuable tool for the study of the confinement effect at the molecular level. Atomistic Monte Carlo (MC) and molecular dynamics (MD) simulations have been used in the past for the study of confined molecular liquids. Layering was also observed in detailed molecular dynamics simulations of liquid benzene between two graphite surfaces,^{8,9} although in this case the first layer adsorbs with an orientation parallel to the surface. Clearly, the structure and extent of the layering depends on the interaction with the surface. More recently, atomistic grand canonical Monte Carlo (GCMC) studies of the behavior of benzene on fully and partially hydroxylated silica planar surfaces have showed that the orientation of benzene at the surface is different for the two surface terminations.¹⁰ For the fully hydroxylated surface, the benzene

Received: January 12, 2011

Revised: June 14, 2011

Published: June 23, 2011

forms layers at the surface with the first layer oriented perpendicular to the surface. For the partially hydroxylated layer, the first layer does not have strong orientational order. For both surfaces, the second adsorbed layer has almost no orientational order.

The interaction of a benzene molecule with various surfaces has been studied using density functional theory (DFT) and the adsorption energy depends not only on the material but also on the surface structure. For example, on Al(111) there is no binding,¹¹ whereas on transition metal surfaces such as Ni(111) or Pt(111) the benzene binds strongly with adsorption energies of 96 and 117 kJ mol⁻¹, respectively.^{12,13} Furthermore, on the Ni(110) surface benzene has an even higher adsorption energy of 205 kJ mol⁻¹.¹² The presence of O on the Al(111) surface increases the adsorption energy of benzene but on α -Al₂O₃(0001) the benzene does not bind to the surface.¹¹ On the Si(001)-(2 × 1) surface benzene undergoes a cycloaddition reaction, but if the same surface is passivated with hydrogen there is almost no interaction between the benzene and the surface.¹⁴ It should be noted that these calculations exclude the effect of van der Waals (vdW) forces, which can be important in some systems. For the Si(001)-(2 × 1) surface the vdW forces change the relative energetic ordering of different adsorption structures.¹⁵ For benzene on graphite¹⁶ or benzene on Au(111),¹⁷ the interaction is significant and is almost entirely due to vdW forces.

In summary, to understand fully and predict the behavior in the confined system, it is essential to understand the interaction of the liquid with the specific surface and to remove the uncertainty in the interface structure. To achieve this ab initio calculations are of particular importance. In this work we use a dualscale modeling approach and consider benzene adsorbed on gold, which is unreactive, has a well-defined (111) surface structure and interacts strongly with benzene. Specifically, we study benzene liquids confined between two parallel gold surfaces using a systematic hierarchical simulation methodology, which combines density functional theory (DFT) with classical atomistic molecular dynamics simulations. Our primary goal is to study the effect of confinement on the structural and dynamical properties of benzene, for a variety of systems, using a realistic atomistic force field, developed from accurate ab initio calculations, capable of predicting various adsorption sites and molecule orientations.

In section 3 we present DFT calculations of benzene on the gold (111) surface, using the van der Waals density functional (vdW-DF) to describe vdW interactions.^{18–20} These results are used to build a classical atomistic force field for the surface interaction of benzene with gold. The force field is described in section 4, and the atomistic adsorption curves are compared to the DFT results. The properties of liquid benzene layers of various thicknesses confined between two gold surfaces are presented in section 5. Finally, our findings and conclusions are summarized in section 6.

2. METHOD

DFT Calculations. Density functional theory calculations were performed using the VASP code.^{21–24} This code employs a plane wave basis set to describe the valence electrons and projected augmented waves (PAWs) to describe the core electrons.^{25,26} A plane wave cutoff energy of 400 eV (38.6×10^3 kJ mol⁻¹) was chosen. The code was modified so that vdW interactions were included via a self-consistent implementation of the vdW-DF functional.^{18–20} Although this functional does not have the correct long-range asymptotic behavior of the energy as a

function of distance for metals, since screening effects are not taken properly into account, the energy and structure at the equilibrium position should be accurate. The vdW-DF calculations were performed using Perdew–Burke–Ernzerhof (PBE) exchange.^{27,28} The lattice constant of bulk, fcc Au was found to be 4.23 Å, which is close to the value of 4.26 Å used by Mura et al.²⁹ This is larger than the lattice constant of 4.17 Å that is obtained using the PBE generalized gradient approximation without vdW, which could be due to the fact that, although the vdW-DF functional describes long-range interactions better than PBE, the short-range interaction may be described less well. Even so, it overestimates the experimental value of 4.08 Å by less than 4%.

The gold (111) surface has a hexagonal unit cell with dimensions $a = b = 2.99$ Å and $c/a = 8(3/2)^{1/2}$. The convergence of the results with respect to number of atomic layers was checked, and even though van der Waals are long-range, extending the slab to 7 atomic layers makes no significant change to the results. The artificial dipole due to the asymmetry of the slab was also checked, and neither increasing the cell size perpendicular to the surface from $8(3/2)^{1/2}a$ to $12(3/2)^{1/2}a$ (29.3 to 43.9 Å) nor using the dipole correction changed the results significantly; that is, the change in adsorption energy is less than 0.02 eV (1.93 kJ mol⁻¹). For the adsorption calculations a surface of 4×4 times the unit cell was used, which corresponds to a coverage of 0.0625 monolayers. A Brillouin zone mesh of $4 \times 4 \times 1$ was used (equivalent to $16 \times 16 \times 1$ for a surface unit cell). The bottom two layers were kept fixed during the geometry relaxation process and the relaxations were terminated when the maximum force on any atom was less than 10 meVÅ⁻¹ (<0.96 kJ mol⁻¹ Å⁻¹).

Atomistic MD Simulations. The classical atomistic molecular dynamics simulations were performed using the GROMACS code.^{30–32} The stochastic velocity rescaling thermostat³³ with a coupling constant of 0.2 ps was used to keep $T = 300$ K. A time step of 1 fs was used, and all of the simulations were run for 100 or 200 ns, after equilibration. The force field parameters for benzene were taken from Jorgensen et al.³⁴ This force field was developed to reproduce properties of liquid benzene, including the density.

In the classical simulations the surface is represented by an array of fixed particles placed in the ideal positions of bulk gold. For the classical simulations the experimental lattice constant of 4.08 Å was used. This fixed particle approximation should not affect the results of the simulation since the mean square displacement for gold atoms at 300 K is only 0.0188 Å².³⁵ Periodic boundary conditions were used in all directions so that the benzene molecules also interact with the bottom of the gold surface in the image cells. The thickness of the slab (7 atomic layers) is ~ 1.41 nm, which is greater than the vdW cutoff length of 1.0 nm, so the benzene molecules will not interact with benzene molecules in image cells in the z direction. The electrostatics are summed in the x and y directions only using the PME method. The lateral dimension of the surface is $a = 4.616$ nm, corresponding to 16×16 surface unit cells along the a and b directions. For the benzene film with two gold interfaces, the Berendsen barostat kept the pressure at 1 atm with pressure coupling in the z direction only.

3. ADSORPTION OF A BENZENE MOLECULE ON Au(111)

Here we present results from the ab initio DFT calculations of a single benzene molecule adsorbed on a Au(111) surface. For the adsorption calculations a low coverage of 0.0625 monolayers was used to avoid the interaction between benzene molecules.

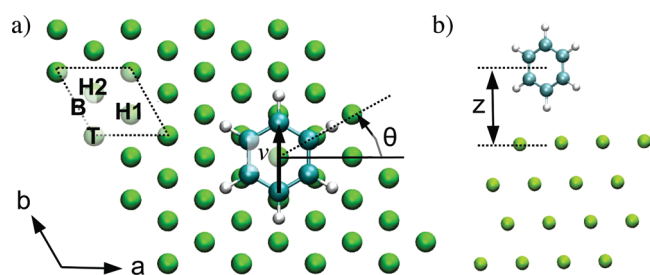


Figure 1. (a) Au(111) surface showing a benzene molecule in a flat orientation on the fcc hollow site, H2, with angle $\theta = 30^\circ$. The T, B, H1, and H2 labels show where the center of the molecule would be for top, bridge, and the hcp and fcc hollow sites, respectively, and the parallelogram indicates a surface unit cell. The vector v , which connects two opposite carbons along the plane of the benzene molecule, is used later in the structural analysis. (b) Benzene oriented vertically above a hollow site. For both flat and vertical orientations the distance, z , is calculated from the center of the benzene molecule to the top of the surface.

Figure 1 shows the adsorption sites on the Au(111) surface. The top site (T) is above a surface atom, the bridge site (B) is midway between adjacent top sites and the hcp and fcc hollow sites (H1 and H2) are situated in the midpoint of three top sites, as shown in Figure 1. Geometry relaxations were carried out at each high-symmetry site of the Au(111) surface. The difference in structure and energy between the two hollow sites is negligible so from now on we consider only the H1 site and refer to it as the hollow site (H).

The adsorption energy, E_{ads} , is defined as $E_{\text{ads}} = E_{\text{bnz}} + E_{\text{surf}} - E_{\text{tot}}$ where E_{tot} , E_{bnz} , and E_{surf} are the energies of the whole system, the isolated benzene molecule, and the isolated surface, respectively. The distance z is calculated from the center of the benzene molecule to the top of the surface slab, as shown in Figure 1b, and we define z_{ads} to be the distance at the energy minimum for each configuration. θ is defined to be the angle between one of the C–H bonds and the a axis, and θ_{ads} is the angle corresponding to the minimum energy configuration.

The lowest energy adsorption structures and energies for each site are shown in Table 1. As we can see, the adsorption energy is slightly larger for the hollow site than the bottom and top sites. However, the differences between the different sites are rather small, implying that the surface does not have a strong site dependence for the benzene molecule. For the hollow and bridge sites the benzene molecules are oriented so that one of the C–H bonds makes an angle $\theta_{\text{ads}} = 30^\circ$ with the x -axis (or crystallographic a axis), as shown in Figure 1. On the top site the benzene prefers an orientation with the C–H bond parallel to the crystallographic a or b axis; that is, $\theta_{\text{ads}} = 0$. The binding distance is 3.22 Å for the bridge and hollow sites, whereas for the top site it is slightly larger (3.34 Å). The value of 3.22 Å is in very good agreement with the results of McNellis et al.,³⁶ who used the method of Tkatchenko and Scheffler (TS).³⁷ These values are about 10% smaller than the value of ~ 3.6 Å,¹⁷ which was obtained from DFT+D results that neglected vdW forces for the structural optimization and hence overestimate the binding distance.

Often vdW forces are neglected, since they are considered weak in comparison to chemisorption energies, and DFT calculations without vdW forces show little or no bonding with gold.^{17,39,40} However, it is clear from the adsorption energies that there is a strong interaction between benzene and gold, which is almost entirely due to vdW forces. This is not surprising since

Table 1. Adsorption Sites, Angles θ_{ads} , Distances z_{ads} , and Energies for Benzene with 0.0625 ML Coverage for Various DFT Calculations (vdW-DF, TS, and DFT+D) and an Experimental Temperature-Programmed Desorption (TPD) Study^a

site	θ_{ads} ($^\circ$)	z_{ads} (Å)	E_{ads} (kJ mol ⁻¹)	method
T	0	3.34	74.9	vdW-DF
B	30	3.22	81.0	vdW-DF
H	30	3.22	82.1	vdW-DF
H	30	3.25	77.2	TS ³⁶
H		3.6	73.3	DFT+D ¹⁷
			61.8	TPD ³⁸

^aThe present results are labelled vdW-DF. The DFT+D method included dispersion forces for the adsorption energy but the adsorption structure was obtained from PW91 calculations, hence the large adsorption distance.

both the benzene molecule and the gold have relatively high polarizabilities. The vdW-DF adsorption energy is in good agreement with both the TS³⁶ and the DFT+dispersion (DFT+D) methods.¹⁷ All of these values are about 25% larger than the experimental value of 61.8 kJ mol⁻¹,³⁸ obtained from a temperature-programmed desorption (TPD) study. However, the accuracy of the experiment is unknown, and it is possible that the adsorption energy could be underestimated due to surface roughness, impurities, etc. All of the results are shown in Table 1.

4. FORCE FIELD FOR BENZENE ON Au(111)

The second part of our hierarchical simulation approach, that combines the methods from the quantum and classical levels of description, involves the development of an accurate classical atomistic force field for the benzene-gold interaction. As mentioned before, many classical simulations use force fields for surface interactions that were parametrized for bulk rather than for interfacial systems or that used DFT calculations that neglected vdW forces.³⁹ As shown in the previous subsection, the vdW forces are substantial and should not be ignored for the benzene-gold system studied here. Thus, in order to develop an accurate classical force field, we use the data from the ab initio calculations, presented in the previous section.

For the classical simulations we use a model in which all surface (Au) atoms are presented explicitly. Then, we obtain pair potentials for the molecule-surface interaction (in our case Au–C and Au–H) using the detailed DFT data. Different functional forms can be used for the pair intermolecular potentials. A common choice is the typical Lennard-Jones (LJ) 12–6 potential of the form

$$V_{\text{LJ}}(r_{i,j}) = 4\varepsilon_{i,j} \left\{ \left(\frac{\sigma_{i,j}}{r_{i,j}} \right)^{12} - \left(\frac{\sigma_{i,j}}{r_{i,j}} \right)^6 \right\} \quad (1)$$

where ε is the depth and $r_0 = 2^{1/6}\sigma$ is the position of the minimum of the LJ potential. Alternatively, a more detailed pair potential such as the Morse potential can be used to describe the molecule-surface interaction

$$V_{\text{Morse}}(r_{i,j}) = \varepsilon_{i,j} [\exp(-2\alpha_{i,j}(r_{i,j} - r_{0i,j})) - 2\exp(-\alpha_{i,j}(r_{i,j} - r_{0i,j}))] \quad (2)$$

where the minimum of the potential has a depth of ε at a distance $r = r_0$. The parameter α determines the shape/width of the

Table 2. Parameters for Four Different Force Fields for Benzene on the Au(111) Surface^a

	Au–C		Au–H	
	σ (nm)	ϵ (kJ/mol)	σ (nm)	ϵ (kJ/mol)
tff _{LJ}	0.346	1.52	0.2747	0.1733
hff _{LJ}	0.321	2.15	0.2747	0.1733

	Au–C			Au–H		
	r_0 (nm)	ϵ (kJ/mol)	α (nm ⁻¹)	r_0 (nm)	ϵ (kJ/mol)	α (nm ⁻¹)
tff _M	0.4104	0.9264	10.1369	0.4006	0.3086	11.6609
hff _M	0.3925	1.0265	10.0693	0.3941	0.3873	11.7284

^aThe tff_M force field was used for the molecular dynamics simulations.

potential. For both potentials the indices i and j denote the atom types (in this case i is an Au atom and j is a C or H atom).

Our goal is to find the set of nonbonded parameters that best describe the DFT data, i.e. adsorption energies. This is not a trivial numerical problem, since it involves a fitting over a many-parameter space. To achieve this we use an optimization algorithm, which is based on simulated annealing (SA). The parameters of the nonbonded interaction are chosen in order to minimize a target cost function. The cost function is defined as the difference between the quantum and classical molecule-surface interaction energies, for all distances and all different configurations (various adsorption sites and orientations) as:

$$F = \sum_{i=1}^{n_{\text{confs}}} \sum_{j=1}^{n_k} \{ [E_{\text{ads}}^{\text{DFT}}(i, z_j) - E_{\text{ads}}^{\text{A}}(i, z_j)]^2 W(i, z_j) \} \quad (3)$$

where the first sum is over all possible different configurations (in this case, adsorption sites and molecule orientations), n_{confs} , and the second is over all different distances per configuration, n_k . z_j is the molecule distance from the surface. $E_{\text{ads}}^{\text{DFT}}(i, z_j)$ is the adsorption energy taken from the detailed ab initio calculations for a specific configuration and molecule distance from the surface, whereas $E_{\text{ads}}^{\text{A}}(i, z_j)$ is the classical adsorption energy of the same configuration using a particular set of nonbonded interaction parameters. $W(i, z_j)$ are weights used to distinguish the importance of various data points in the optimization procedure. In the next paragraphs we show several parametrizations based on different molecular conformations of the benzene molecules and on the two different types of nonbonded pair interactions. Note that the DFT data for the hollow and bridge sites are very similar, and thus, we parametrized the classical force field only for the top and the hollow adsorption sites.

LJ-Based Force Fields. The first two parametrizations considered here use LJ pair potentials and fit the C–Au parameters, $\epsilon_{\text{Au,C}}$ and $\sigma_{\text{Au,C}}$, to reproduce the minimum of the hollow or top flat configuration. The Au–H parameters are taken from the universal force field (UFF).⁴¹ The resulting force fields are referred to as hff_{LJ} and tff_{LJ}. The best set of data for the hff_{LJ} and tff_{LJ} parametrizations are shown in Table 2 and Figure 2a,b. Note that it is not possible to find a set of LJ parameters to describe all DFT data (molecule-surface distances) for each adsorption site; thus the weights, $W(i, z_k)$, in the cost function were adjusted so that the obtained force field reproduced better the DFT position and depth of the minimum.

In both hff_{LJ} and tff_{LJ} cases the agreement between the DFT data and the classical data for the flat configuration is reasonably

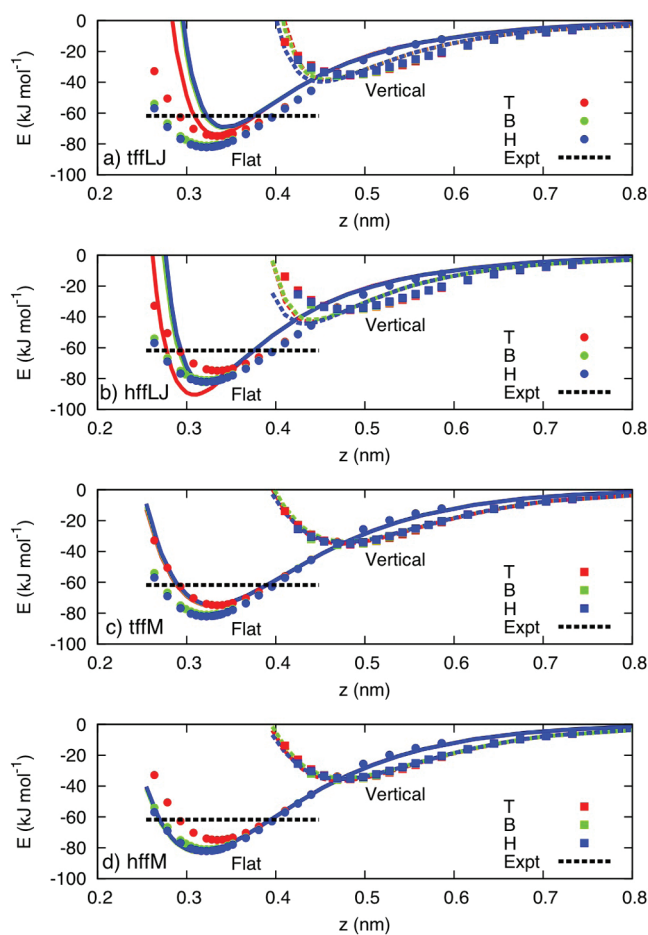


Figure 2. Comparison between the force field adsorption energy curves and DFT results using a LJ interaction fitted to (a) top–flat orientation (tff_{LJ}) (b) hollow–flat orientation (hff_{LJ}), and a Morse interaction fitted to (c) top–flat and top–vertical orientations (tff_M) and (d) hollow–flat and hollow–vertical orientations (hff_M).

good at the minimum of the interaction as well as for longer distances. However, there are discrepancies in the short-range repulsive regime where the LJ based atomistic potential is too steep in comparison with the DFT data. We also observe that the hff_{LJ} parametrization, Figure 2b, overestimates the energy for distances close to the well depth adsorption energy by ~ 10 kJ mol⁻¹ and the energetic ordering of the various configurations predicted by the force field is not the same as for the DFT calculations. However, as mentioned above, the energetic differences between the various configurations are rather small.

To check the transferability of the parameters obtained by fitting to the flat configurations, which have the lowest energy, we compare the energy versus distance curves for benzene in vertical orientations, as shown in Figure 1b. Although the angular dependence of the adsorption energy has not been explicitly calculated, the energy as a function of angle will be smoothly varying since the interaction is purely due to van der Waals interactions and there is no chemical bonding present. The curves are shown in Figure 2a,b and the agreement is reasonable. However, we can see that for both force fields there are some deviations between the DFT data and the atomistic interaction, especially at short distances. This is a clear indication that the typical LJ 12-6 pair potential is not the best choice for describing

the interaction between molecules and surfaces. Furthermore the use of LJ based potentials with different power laws, such as LJ 10-4 or 9-3 potentials, is not physically justified in our case since we are fitting an atom–atom pair potential and LJ 10-4 or 9-3 correspond to integrations of the 12-6 over a plane and semi-infinite slab, respectively. Therefore we decide to fit our DFT data onto a Morse type potential, whose shape can also be modified.

Morse-Based Force Fields. In the second set of parametrizations nonbonded Morse potentials were used, and the values of ε_{ij} , α_{ij} , and r_{0ij} were obtained by minimizing the cost function, F (see eq 3), for the hollow site, denoted “hff_M” or the top site, denoted “tff_M”. In this parametrization we optimized both the C–Au and the H–Au pair potentials and fit to both the vertical and flat configurations. The best set of data for the hff_M and tff_M parametrizations are shown in Table 2 and in Figure 2c,d. Note that in this case, in the minimization of the cost function, we use the same value for all weights, i.e., $W(i, z_k)=1$ for all configurations.

As we can see the agreement between the classical and the ab initio molecule–surface interaction energies is very good for the entire range of distances studied here. This is a clear indication that a Morse interaction potential, whose shape and width can be modified, is a better choice than an LJ potential for describing the complicated many-body molecule–surface interactions in the classical level as pair atom–atom ones. Furthermore, it is very important to note that the different molecule orientations i.e. flat and vertical, are well described, as we can see from Figure 2c,d. The agreement between the DFT data and the classical data for the different orientations is excellent for both hff_M and tff_M cases.

Table 3. Summary of the Four Different Benzene Films, Labelled S1–S4, and Bulk Benzene^a

name of model system	S1a	S1b	S2	S3	S4	B
number of molecules	128	128	256	512	1024	256
film width (nm)	1.17	1.18	2.09	4.18	8.36	–
ρ_{ave} (g cm ⁻³)	0.77	0.76	0.86	0.86	0.86	0.85

^aNote, two structures for the S1 system were observed. The average film widths and average densities, ρ_{ave} (g cm⁻³) are presented. Error bars in density are about ± 0.02 g cm⁻³.

Finally, we should state that it is not possible to find a set of nonbonded interaction parameters that describe at the same time all the different adsorption sites, i.e., top, bridge, and hollow. This is not surprising taking into account that the classical pair atomistic potentials neglect electronic overlap and relaxation. Since the differences in energy between the top and hollow configurations are anyway small, we have arbitrarily chosen to use the tff_M parametrization for the molecule–surface interaction in the molecular dynamics simulations in the following section.

5. LIQUID BENZENE CONFINED BETWEEN TWO Au(111) SURFACES

In this section we present results from classical all-atom MD simulations about the density, structure and dynamics of confined benzene systems. We have simulated four different systems (S1–S4, see also Table 3) with 128, 256, 512, and 1024 benzene molecules between two parallel Au(111) surfaces as well as a bulk benzene liquid (B) with 256 molecules. In all cases $T = 300$ K and $p = 1$ atm. Simulation times vary from 100 to 200 ns. In Figure 3 we present typical snapshots, taken from the MD simulations, for each film. For the S1 system two distinct structures were observed.

Density. Various characteristics of the films are shown in Table 3. The averaged film thicknesses of the model systems studied here, are approximately 1.17, 1.18, 2.09, 4.18, and 8.36 nm for S1a, S1b, S2, S3, and S4, respectively. The widths are defined as the average box height minus the thickness of the gold slab (1.41 nm). Note that these thicknesses correspond to about 2.4, 2.4, 4.2, 8.4, and 17.2 molecular diameters, respectively. A clear layering is seen at the interfaces for all systems. In the two thinner films, S1 and S2, the layers are visually distinct, with the S2 film having five distinct layers and the S1 film having two distinct layers. In addition the smallest film exhibits two different stable configurations, shown in Figure 3a,b, and an additional ordering along the crystallographic directions. In contrast the two bigger systems S3 and S4 show a clear ordering only for the first layer whereas at longer distances from the surface a more bulk-like behavior is seen. Overall, the strength of the confinement varies from bulk-like to very confined, highly ordered systems.

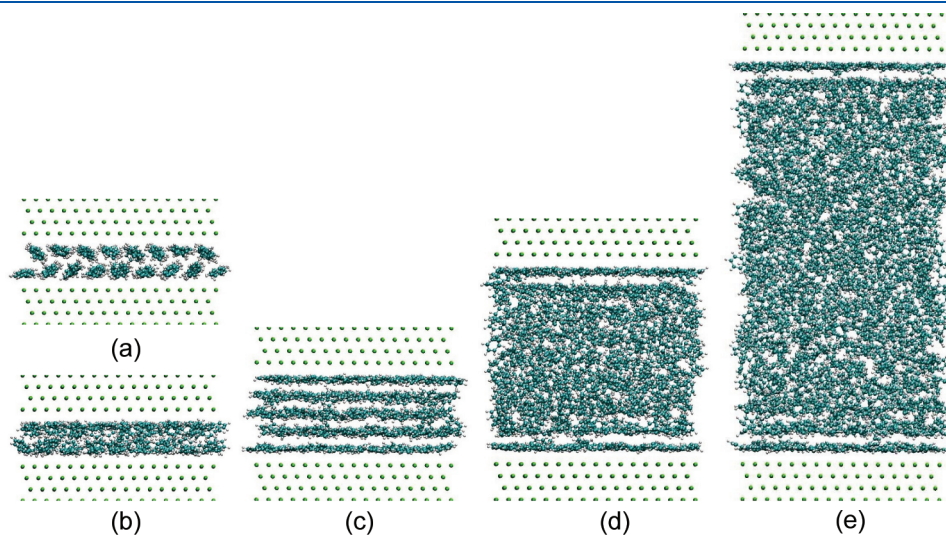


Figure 3. Snapshots of benzene films of different thicknesses: (a,b) S1, (c) S2, (d) S3, and (e) S4.

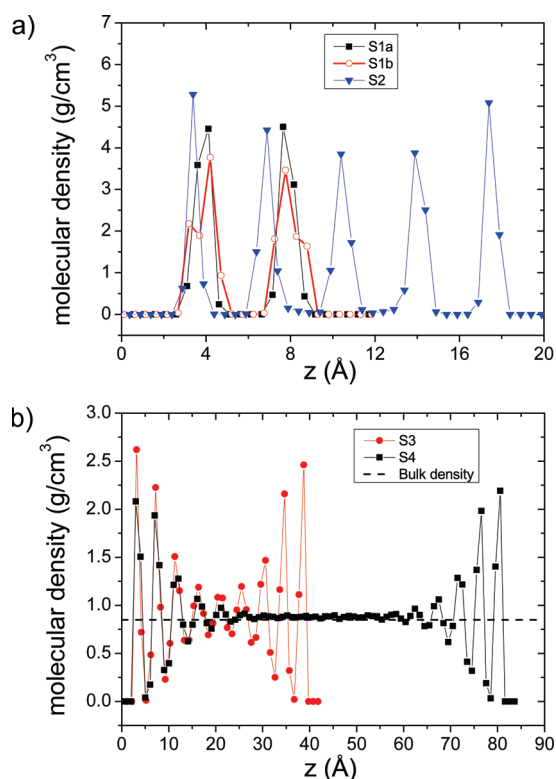


Figure 4. Time averaged molecular density profiles for (a) S1a, S1b, and S2 films and (b) S3 and S4. The horizontal dotted line denotes the density value of the bulk benzene (B system).

In the next stage, an analysis of the systems along the direction of confinement (z direction) has been performed by dividing the space into bins separated by parallel x – y planes of width of 0.5 Å for the two thinner films (S1 and S2) and 1.0 Å for the S3 and S4 films. Structural and conformational properties were obtained by averaging over all configurations obtained from the MD runs.

The time-averaged molecular (center-of-mass) density profiles, $\rho(z)$, as a function of the distance from the metal surfaces (z -direction) of the model films studied here, are shown in Figure 4. In Figure 4a the $\rho(z)$ for the two thinner films (S1 and S2) are presented. As was also clear from the snapshots of the atomistic simulations (see Figure 3a–c), the structures show two and five clear layers, respectively, with the contact layers being the most strongly peaked. In these two films the layers are well separated with the density going to zero between each layer. As expected the density profiles are symmetrical with respect to the center of the film. Furthermore, the smallest film exhibits two different stable configurations with slightly different density profiles, shown with squares and circles in Figure 4a. The energetic difference between these two configurations is very small (about 200 kJ/mol) with the first one, (a), having the lower energy.

In Figure 4b, the $\rho(z)$ for the two thicker films (S3 and S4) are presented. For these larger systems we observe the typical oscillatory profile characteristic of fluid–solid interfacial systems. The density has clear peaks near to the solid surfaces with their height decreasing as the distance from the surface increases. The density almost goes to zero only between the contact and second layers. For the S3 system the corrugation in the density continues into the center of the film, showing nine layers. In contrast the largest system (S4) exhibits a clear bulk-like region in the

center of the film with the density equal to the bulk density ($\rho_0 = 0.85 \text{ g cm}^{-3}$ at $T = 300 \text{ K}$, $p = 1 \text{ atm}$). Overall, the effect of the interface on the density profiles extends ~ 2.5 – 3.0 nm from the gold surface.

The contact layers have peak densities ranging from about $2.6\rho_0$ for the largest film (S4) up to almost $6.4\rho_0$ for the S2 film. For all but the thinnest film, the first peak appears about 3.8 Å from the highly attractive Au surface. For the thinnest film the peak is slightly shifted to a distance of 4.2 Å. The reason for this shift is due to the different orientation of molecules in this film (see also snapshots in Figure 3a,b). The different structure of the smallest film can also be seen from the slightly larger spacing and lower peak value of the contact layers compared those of the S2 film.

The average density of each film as well as the density of the contact layers are shown in Table 3. Despite the fact that the contact layers are denser than the bulk, the S1 film has an overall density that is lower than the bulk value, which is due to the high orientational ordering of this film. A lowering of the density was observed for benzene confined in a silica pore of width 2.4 nm.¹ This is consistent with the strong layering observed in GCMC simulations of benzene in silica nanopores.¹⁰

Finally, we should state that close to the interface there is a clear competition between orientation and density (packing optimization). This is clearest for the thinnest film, S1. In this system there are not enough molecules to form three layers but too many to form two flat layers. This results in a different orientation of the molecules to account for the extra molecules in the two layers. This can also give rise to ordering along the a and b crystallographic directions, which can be seen in Figure 3a. Note that the MD simulations presented here were performed under NPT conditions. This is different than typical experiments in nanopores with fixed volume. It should also be mentioned that the force field for benzene is parametrized to reproduce properties of the liquid phase and not for the solid phase. Thus it is questionable how well the properties of the crystalline phase of benzene are reproduced. This will be further examined in future work concerning the effect of confinement as a function of temperature.

Structure. The orientational order of the confined benzene molecules is also of particular interest. The main question here is related with molecular orientation tendencies induced by the confinement. The orientation of a molecule can be quantified by calculating the second rank order parameter. For an arbitrary vector, along the molecule, \mathbf{v} , this is defined as

$$P_2(\cos(\theta)) = \frac{3}{2} \langle \cos^2(\theta) \rangle - \frac{1}{2} \quad (4)$$

where θ is the angle of the vector \mathbf{v} with the z coordinate axis, i.e., in our case normal to the surface, and $\langle \dots \rangle$ denotes the ensemble average of all molecules in the system. Here, in order to analyze the orientation of the entire benzene molecule, we choose as \mathbf{v} the vector connecting the two opposite carbons along the plane of the molecule (see Figure 1a). The limiting $P_2(\cos(\theta))$ values of -0.5 , 1.0 , and 0.0 corresponds to the benzene oriented parallel to the surface, perpendicular to the surface and random orientation respectively.

$P_2(\cos(\theta))$ data for the two bigger systems (S3 and S4) are shown in Figure 5a. It can be clearly seen that the profile of $P_2(\cos(\theta))$ oscillates, resembling very much the profile of the local mass density distribution discussed in the previous section. Next to the Au surfaces $P_2(\cos(\theta))$ attains negative

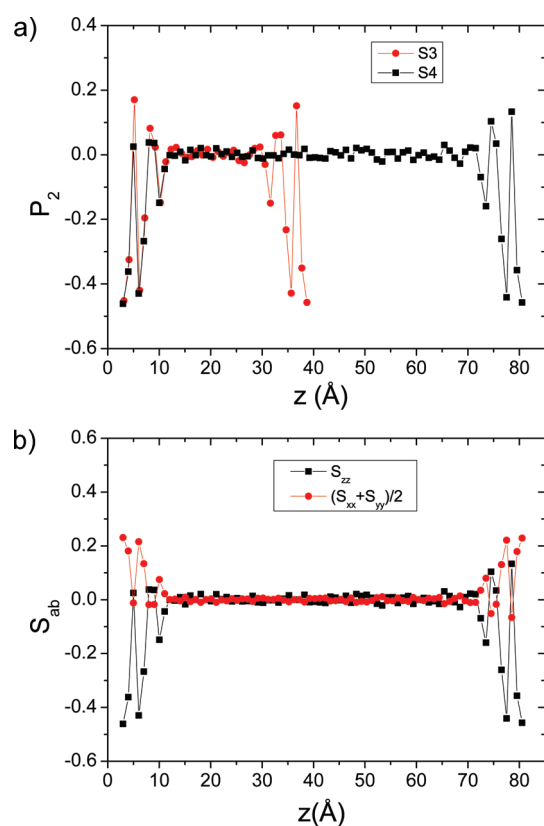


Figure 5. (a) Orientational order parameter $P_2(\cos(\theta))$ for systems S3 and S4 and (b) components of the Saupe matrix S_{zz} ($S_{xx} + S_{yy}$)/2 for system S4.

values (e.g., $P_2(\cos(\theta)) = -0.45$ at a distance of ~ 3.2 Å), indicating the strong tendency of the benzene molecules to orient parallel to the surface plane. The characteristic oscillatory profile of the $P_2(\cos(\theta))$ order parameter for the larger system (S4) extends to distances of about 2 nm in rough agreement with the density profile (see Figure 4b). Beyond this, in the middle of the film, $P_2(\cos(\theta))$ becomes 0.0, which is characteristic of random orientation. The case of the two thinner films, S1 and S2, is different. For these systems the values of $P_2(\cos(\theta))$ are negative at distances at which density profiles exhibit clear peaks (see Figure 4a) but do not exist in between the layers, because there the density is zero.

To further analyze the orientation of benzene molecule we have calculated the average values of the second rank order parameter for each adsorption layer, $P_2^{\text{ads}}(\cos(\theta))$. Each adsorption layer is defined as the distance between two consecutive minima in the density profiles, taking into account the symmetry with respect to the center of the film. Thus, S1 has one, S2 has three, S3 has five and S4 has six adsorbed layers. The data are shown in Table 4. We have also averaged the data taking into account the symmetry along the middle of the film. $P_2^{\text{ads}}(\cos(\theta))$ of the first adsorbed layer is negative for all systems, showing the tendency of molecules very close to the surface to be parallel to the gold surface plane. It is clear that this tendency is very strong for S2, S3 and S4 films (values of $P_2^{\text{ads}}(\cos(\theta))$ are between -0.45 and -0.41), in which all benzene molecules in the first adsorption layer are almost perfectly parallel with the Au plane. For the S2 system this orientation extends into the second and third adsorbed layer. In contrast, the two bigger systems show a much smaller tendency for the second layer and an average random orientation for all the

Table 4. Values of $P_2^{\text{ads}}(\cos(\theta))$ in Each Adsorbed Layer of the Various Films^a

layer	S1a	S1b	S2	S3	S4
1	-0.224	-0.218	-0.45	-0.42	-0.41
2			-0.35	-0.14	-0.13
3			-0.33	-0.02	-0.01
4				0.00	0.00

^aThe values are averaged over the two surfaces and the error bars are ± 0.02 . The value in the bulk is 0.0.

adsorbed layers after the second one. The thinnest film (S1 system) has only one adsorbed layer on each surface, in which the molecules have a slightly modified orientation because of the excess number of molecules (see also the previous section).

Next, we analyze the uniaxial (or otherwise) character of the anisotropy exhibited in the benzene molecules. To achieve this we have calculated all the components of the traceless, symmetric Saupe matrix S , which is defined as

$$S_{ab} = \frac{3}{2}\langle l_a l_b \rangle - \frac{1}{2}\delta_{ab} \quad (5)$$

where l_a , $a = x, y, z$, is the direction cosines relating the vector \mathbf{v} to the Cartesian coordinate frame and δ_{ab} is the Kronecker delta function. For molecular phases characterized by uniaxial anisotropy along the z direction, $S_{xx} = S_{yy} = -1/2S_{zz}$ whereas all of the off-diagonal elements should be zero. Data for the diagonal elements of the Saupe matrix for the bigger system (S4) are shown in Figure 5b. Within the statistical accuracy the uniaxial conditions are identically satisfied in the two interfacial regions. The same is also true for the other systems.

Dynamics. In the final part of the analysis of the confined benzene fluid, we study the effect of the confinement on the dynamics of the benzene molecules. Although the thermostat coupling constant of 0.2 ps is smaller than some of the dynamical correlation times it has been shown for water that the diffusion times are not significantly altered.³³ First, we check the orientational relaxation of the benzene molecules. A standard way to analyze the segmental-orientational dynamics of molecules is through time correlation functions of a vector \mathbf{v} . The reorientation of such a vector can be studied by considering ensemble averaged Legendre polynomials of the inner product of the unit vector parallel to \mathbf{v} at time $t = 0$ and $t = t$. The most typical is the second Legendre polynomial, which is directly related with the second bond order parameter discussed above, defined as

$$P_2(t) = \frac{3}{2}\langle \cos^2(\theta(t)) \rangle - \frac{1}{2} \quad (6)$$

with θ now being the angle of the vector \mathbf{v} at time t relative to its original position. Here, we again choose \mathbf{v} to be the vector connecting the two carbons along the plane of the molecule (see Figure 1). Data for the autocorrelation functions (ACFs) of $P_2(t)$ as a function of distance from the surface planes give information about the dependence of the orientation dynamics as a function of distance from the solid surfaces.

In Figure 6a we present $P_2(t)$ of the benzene molecules, belonging to different adsorption layers, defined by the minima in the density profiles (see also the previous section), for the bigger system studied here, S4. Also shown in the figure is the corresponding bulk $P_2(t)$ profile. It is obvious a qualitatively different picture for the different sets of data. In more detail $P_2(t)$

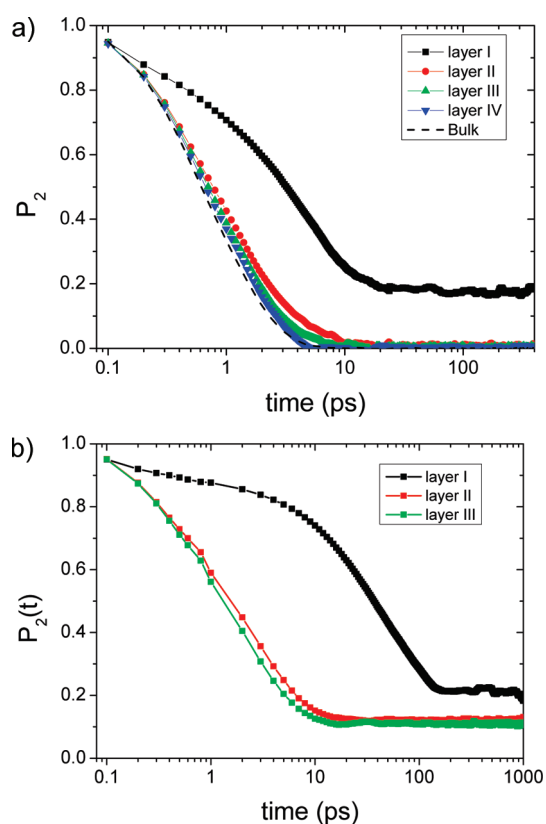


Figure 6. Time autocorrelation functions of $P_2(t)$, analyzed layer-by-layer, for the (a) S4 and (b) S2 system.

of all but the first adsorbed layers gradually go to zero at long times, denoting complete decorrelation. In contrast $P_2(t)$ of the first adsorbed layer exhibits slowly decreasing decorrelation for short times and a constant plateau value of ~ 0.2 after about 20 ps. We also observe that in the first adsorption layer the molecular orientation dynamics is slower than in the bulk and also than in the other adsorption layers. The dynamics of molecules belonging to the second and third adsorption layers is slightly slower than in the bulk, whereas the dynamics of all other adsorption layers is indistinguishable from that observed in bulk benzene.

It is quite common to fit the long time regime of such autocorrelation functions with modified stretched exponential Kohlrausch–Williams–Watts (KWW) functions⁴² of the form $P_2(t) = A \exp(-(t/t_{\text{KWW}})^\beta)$, where t_{KWW} is a characteristic relaxation time and β is the stretch exponent accounting from deviation from the Debye behavior. A is a pre-exponential factor that takes into account relaxation processes (such as bond and angle vibrations) at very short time scales. The curves of Figure 6a can be accurately fitted with KWW functions for time scales above about 0.5 ps. Especially for the first adsorbed layer only times up to about 100 ps can be fitted since for longer times $P_2(t)$ reaches a constant value. Values for t_{KWW} and β that provide the best fits to the simulation data for all adsorbed layers of system S4 are summarized in Table 5. As we can see the relaxation time of the benzene molecules very close to the gold surfaces (first adsorption layer) is more than five times slower than the bulk value. The relaxation time of the molecules belonging in the second and third adsorption layer is slightly larger (about 20% and 10% respectively) than the bulk one, whereas it attains the bulk value for distances after the third adsorbed layer.

Table 5. Values of Relaxation Time t_{KWW} and Stretching Exponent β , Obtained from Fits of the $P_2(t)$ Time ACFs of the S4 System As a Function of the Distance of the Benzene Molecules from the Gold Surfaces

layer	range (Å)	t_{KWW} (ps)	β
I	0–5	5.80 ± 0.20	0.61 ± 0.05
II	5–10	1.25 ± 0.15	0.79 ± 0.05
III	10–15	1.10 ± 0.15	0.87 ± 0.05
IV	15–20	1.05 ± 0.15	0.92 ± 0.05
V	20–25	1.03 ± 0.15	0.92 ± 0.05
Bulk	–	1.00 ± 0.10	0.93 ± 0.03

The stretch exponent β of the bulk unconstrained fluid is about 0.9, showing small deviations from the ideal (simple exponential) behavior. The value of β is much smaller for the molecules belonging in the first adsorption layer ($\beta = 0.6$) showing a broader, compared to bulk, distribution of relaxation times close to the surface. In agreement with the qualitative picture of the relaxation times, β in the second adsorption layer is also smaller than the bulk value, whereas values of β after the second adsorption layer are very close, within the error bars, to the bulk one. The values of the characteristic relaxation time reported here are also quite similar to recent experimental data of benzene confined in nanoporous sol–gel monoliths.⁵ Overall, the effect of the interface on the orientational dynamics of the bigger systems extends mainly to the molecules next to the surfaces (first adsorption layer), i.e., ~ 5 – 10 Å from the gold surface.

The picture for the S3 film is very similar, both qualitatively and quantitatively. In contrast the dynamics of the two thinner films, S1 and S2, is different. The $P_2(t)$ data for the three adsorption layers of the S2 system are shown in Figure 6b. Note that from now on we do not distinguish between the dynamics of the two different configurations of the smallest film (S1a and S1b), since there is practically no difference. The $P_2(t)$ data of molecules belonging in the first adsorption layer for both S1 and S2 films also exhibit the same anomalous behavior for $P_2(t)$: a slowly decreasing decorrelation for short times and a constant plateau value of ~ 0.2 after about 100 ps. $P_2(t)$ for molecules belonging in the second and third adsorbed layer of the S2 film also reach plateau lower values, of ~ 0.12 and 0.08 respectively after only ~ 10 ps. Note that the anomalous incomplete orientation dynamics of $P_2(t)$ is present during the whole duration of the present runs (200 ns), showing clearly that those systems never really decorrelate for times at least 5 orders of magnitude longer than the relaxation time of the bulk system. This is an important qualitative difference in the dynamics of confined benzene molecules, compared to the bulk films, and is due to the strong degree of confinement.

To further compare the orientational relaxation of the different films we show, in Figure 7, $P_2(t)$ of the molecules next to the gold surfaces (first adsorption layer), for all systems studied here. As stated above, there is a qualitatively similar dynamical behavior for the first adsorption layer of all films, i.e. $P_2(t)$ exhibit clear anomalous dynamics with the appearance in longer times (ranging from 20 ps to about 100 ps) of a plateau value of about 0.2, showing an incomplete relaxation of the molecules. However, we also see that the $P_2(t)$ curve of the S2 system is much slower than those of the two thicker films, S3 and S4, as well as of the thinnest film, S1, even in the short time regime. In more detail, the shape of the S3 and S4 $P_2(t)$ curves for short times

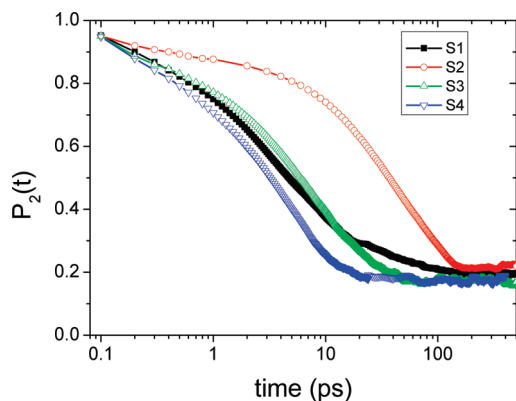


Figure 7. $P_2(t)$ time autocorrelation functions of the molecules next to the gold surfaces (first adsorption layer), for all systems studied here.

(below about 10 ps) are similar, showing behavior similar to curves of bulk unconstrained molecular fluids. Also of importance, is the anomalous form of the $P_2(t)$ data for the S2 system, even at initial times, showing the clearly different behavior of this film, which was obvious from the density and the structural characteristics, as discussed previously.

In the last part of the results section, we discuss the translational dynamics of the confined benzene molecules. This can be quantified through mean square displacement (MSDs) of the molecules center-of-mass, $\langle(R(t) - R(0))^2\rangle$, where $R(t)$ is the position of the center-of-mass at time t . For systems that are confined in one direction it is of interest to measure the translational dynamics in the other two free directions, in this case x and y . In order to examine the dynamics in these two dimensions we calculate the MSDs in the xy plane parallel to the gold surfaces: $DR_{xy}(t) = \langle(R_{xy}(t) - R_{xy}(0))^2\rangle$, where the brackets denote the statistical average over all molecules present in the model systems. Results about DR_{xy} for all the systems studied here are shown Figure 8a. The bulk, as well as the two bigger systems (S3 and S4) exhibit as expected nonlinear anomalous dynamics for short times (up to about 50 ps) and a linear Fickian dynamics at longer times. It is also clear that the xy translational mobility of the two bigger systems is slower, but within the same order of magnitude, than the bulk free dynamics. The behavior of the two smaller, more confined systems, is very different. Both S1 and S2 films are practically frozen, that is, there are only small vibrations of the benzene molecules, of about 0.4 – 0.6 Å.

The above behavior is even more clear if we calculate the time-dependent xy self-diffusion coefficient, defined as

$$D_{xy}(t) = \frac{\langle(R_{xy}(t) - R_{xy}(0))^2\rangle}{4t} \quad (7)$$

Values of $D_{xy}(t)$ for all of the systems studied here are plotted in Figure 8b. As expected, the bulk system shows a time dependent value for the short times whereas it reaches a plateau value (at around 20 – 30 ps) of about $0.25 \pm 0.02 \text{ \AA}^2 \text{ ps}^{-1}$. The two bigger confined films (S4 and S3 systems) exhibit qualitatively similar behavior with plateau, time-independent, values of D_{xy} equal to 0.17 ± 0.03 and $0.08 \pm 0.03 \text{ \AA}^2 \text{ ps}^{-1}$ respectively. Finally $D_{xy}(t)$ of the molecules of both S2 and S1 system show a constant decreasing $D_{xy}(t)$, which is to be expected since the molecules in these systems are practically frozen.

Overall, the translational dynamics of the benzene molecules, confined between two gold surfaces, in the free unconstrained

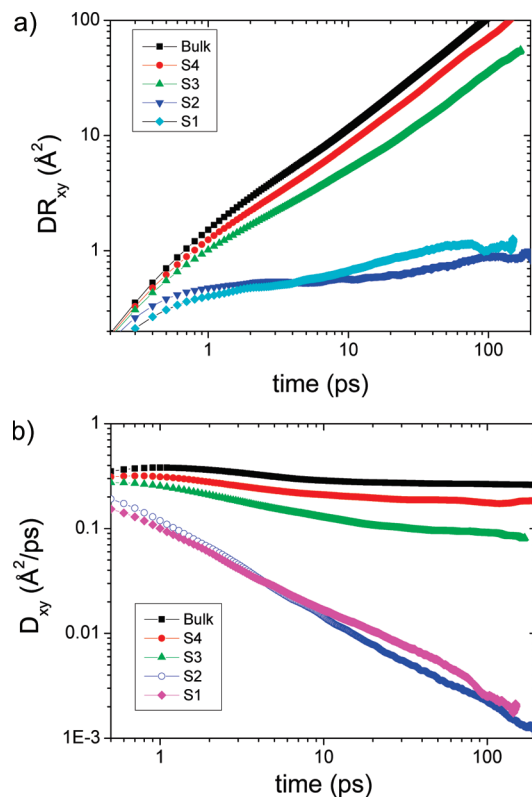


Figure 8. Translational center-of-mass xy dynamics of all confined benzene systems studied here: (a) mean square displacements and (b) time dependent self-diffusion coefficients.

xy plane clearly shows a gradual decrease with the increase of the confinement effect. This decrease in the benzene mobility becomes clearer for systems with about 7–8 molecular diameters range of confinement (as the S3 system studied here), for which the mobility is about 2 times smaller than the bulk one. Finally for even more confined systems, as the S2 and S1 systems (only 2–4 molecular diameters), the translational xy mobility is practically zero.

6. SUMMARY AND CONCLUSIONS

This work reports a hierarchical dualscale study of liquid benzene confined between two gold surfaces at a temperature of $T = 300 \text{ K}$ and $p = 1 \text{ atm}$. DFT calculations of a single benzene molecule adsorbed at different sites on the Au(111) surface were performed. A classical atomistic potential for the interaction of benzene with the surface was developed based on these DFT calculations. This interfacial potential was used in molecular dynamics simulations for liquid benzene films confined between two parallel gold surfaces.

The DFT calculations show a strong adsorption of the benzene molecule on the gold surface. Gold and benzene are both highly polarizable, and the interaction between them is almost entirely due to vdW forces. The adsorption energies on the various surface sites are similar and range between 74.9 and 82.1 kJ mol^{-1} when the benzene molecule is flat on the gold surface. This means that the surface is rather smooth and there is no strong site dependence.

The derivation of a new, accurate classical pair molecule/surface force field, through parametrization of detailed DFT data,

is a major part of this work. Using an optimization algorithm, which is based on simulated annealing, we obtain a set of non-bonded pair C–Au and H–Au parameters that accurately describe the detailed many-body DFT data. Flat and vertical orientations on three adsorption sites (top, hollow1 and bridge) are considered. Several parametrizations using two different types of interaction potentials and fits to different adsorption site data were developed and compared. We found that a Morse potential, whose shape and width can be modified, is a better choice than a Lennard-Jones potential for describing complicated many-body molecule-surface interactions at the classical level as pair atom–atom interactions. The Morse potential parametrizations give good agreement between the DFT and classical data for both flat and vertical molecular orientations.

Four systems with different numbers of benzene molecules were studied using molecular dynamics and the benzene film thicknesses ranged from 1.17 to 8.36 nm corresponding to 2.4 to 17.2 molecular diameters. The density, structure, and dynamics of the benzene films were analyzed. The density displays the typical fluid–solid behavior, and only the thickest film of 8.36 nm has the same density as bulk benzene in the center of the film. In this case the layering near the surface extends approximately 2.5–3.0 nm from the gold surface. For the smallest two films the effect of confinement is strongly pronounced and the benzene liquid exhibits discrete layers throughout the film. The orientation of the benzene molecules in the layers was analyzed and the contact layer for all films shows a strong ordering with the benzene oriented parallel to the gold surface. For the 2.09 nm film this orientational order extends throughout the film whereas for the largest two films the second layer from the surface is less clearly ordered and the third layer becomes already disordered.

To analyze the dynamics of the films the time autocorrelation function $P_2(t)$ for each adsorption layer was calculated. For all the films the layer in contact with the gold surface shows a marked slowing down of the dynamics for short times whereas for longer times $P_2(t)$ never completely decorrelates. For the two largest films the inner layers show a similar decorrelation time as bulk benzene. In the case of the smallest two films the autocorrelation functions for all the layers never completely decorrelate. Overall, it is clear that the effect of confinement changes qualitatively the behavior of films thinner than ~ 4 nm. Above this thickness the influence of the interface does not significantly change the orientational order or dynamics beyond the first layer (approximately 5–10 Å). The translational dynamics of the confined systems in the xy plane parallel to the gold surfaces also show a clear decrease of the mobility as the strength of the confinement increases. This is even more clear for the 2.09 nm confined system studied here where the mobility is more than an order of magnitude smaller than in the free unconstrained system. Smaller, more confined systems are practically frozen.

Future work concerns two directions. The first one is to study the effect of temperature on structure and dynamics for various film thicknesses. The second direction is to extend the present hierarchical approach to investigate and compare the behavior of benzene films on a variety of different surfaces. The study of the confinement effect for different molecule-surface interactions would be of particular importance.

AUTHOR INFORMATION

Corresponding Author

*E-mail: johnston@mmpip-mainz.mpg.de; vagelis@tem.uoc.gr.

ACKNOWLEDGMENT

We thank Andris Gulans for valuable discussions regarding the van der Waals calculations and Davide Donadio and Kurt Kremer for a critical reading of the manuscript. Funding was provided by the DFG SPP1369 Priority Program. We would also thank the referee for his/her constructive comments.

REFERENCES

- (1) Xia, Y.; Dosseh, G.; Morineau, D.; Alba-Simionesco, C. *J. Phys. Chem. B* **2006**, *110*, 19735.
- (2) Watanabe, A.; Iiyama, T.; Kaneko, K. *Chem. Phys. Lett.* **1999**, *305*, 71.
- (3) Alba-Simionesco, C.; Dosseh, G.; Dumont, E.; Frick, B.; Geil, B.; Morineau, D.; Teboul, V.; Xia, Y. *Eur. Phys. J. E* **2003**, *12*, 19.
- (4) Alba-Simionesco, C.; Coasne, B.; Dosseh, G.; Dudziak, G.; Gubbins, K. E.; Radhakrishnan, R.; Sliwinski-Bartkowiak, M. *J. Phys.: Condens. Matter* **2006**, *18*, R15.
- (5) Zhu, X.; Farrer, R. A.; Fourkas, J. T. *J. Phys. Chem. B* **2005**, *109*, 12724.
- (6) Loughnane, B. J.; Scodinu, A.; Fourkas, J. T. *J. Phys. Chem. B* **2006**, *110*, 5708.
- (7) Gelb, L. D.; Gubbins, K. E.; Radhakrishnan, R.; Sliwinski-Bartkowiak, M. *Rep. Prog. Phys.* **1999**, *62*, 1573.
- (8) Winkler, R. G.; Hentschke, R. *J. Chem. Phys.* **1993**, *99*, 5405.
- (9) Clifton, B.; Cosgrove, T. *Mol. Phys.* **1998**, *93*, 767.
- (10) Coasne, B.; Alba-Simionesco, C.; Audonnet, F.; Dosseh, G.; Gubbins, K. E. *Langmuir* **2009**, *25*, 10648.
- (11) Blomqvist, J.; Salo, P. *J. Phys.: Condens. Matter* **2009**, *21*, 225001.
- (12) Mittendorfer, F.; Hafner, J. *Surf. Sci.* **2001**, *472*, 133–153.
- (13) Saeyes, M.; Reyniers, M.; Marin, G. B. *J. Phys. Chem. B* **2002**, *106*, 7489.
- (14) Johnston, K.; Nieminen, R. M. *Phys. Rev. B* **2007**, *76*, 085402.
- (15) Johnston, K.; Kleis, J.; Lundqvist, B. I.; Nieminen, R. M. *Phys. Rev. B* **2008**, *77*, 121404(R).
- (16) Chakarova-Käck, S. D.; Schröder, E.; Lundqvist, B. I.; Langreth, D. C. *Phys. Rev. Lett.* **2006**, *96*, 146107.
- (17) Tonigold, K.; Gross, A. *J. Chem. Phys.* **2010**, *132*, 224701.
- (18) Dion, M.; Rydberg, H.; Schröder, E.; Langreth, D. C.; Lundqvist, B. I. *Phys. Rev. Lett.* **2004**, *92*, 246401.
- (19) Dion, M.; Rydberg, H.; Schröder, E.; Langreth, D. C.; Lundqvist, B. I. *Phys. Rev. Lett.* **2005**, *95*, 109902(E).
- (20) Gulans, A.; Puska, M. J.; Nieminen, R. M. *Phys. Rev. B* **2009**, *79*, 201105(R).
- (21) Kresse, G.; Hafner, J. *Phys. Rev. B* **1993**, *47*, 558.
- (22) Kresse, G.; Hafner, J. *Phys. Rev. B* **1994**, *49*, 14251.
- (23) Kresse, G.; Furthmüller, J. *Comput. Mater. Sci.* **1996**, *6*, 15.
- (24) Kresse, G.; Furthmüller, J. *Phys. Rev. B* **1996**, *54*, 11169.
- (25) Blöchl, P. E. *Phys. Rev. B* **1994**, *50*, 17953.
- (26) Kresse, G.; Joubert, D. *Phys. Rev. B* **1999**, *59*, 1758.
- (27) Perdew, J. P.; Burke, K.; Ernzerhof, M. *Phys. Rev. Lett.* **1996**, *77*, 3865.
- (28) Perdew, J.; Burke, K.; Ernzerhof, M. *Phys. Rev. Lett.* **1997**, *78*, 1396(E).
- (29) Mura, M.; Gulans, A.; Thonhauser, T.; Kantorovich, L. *Phys. Chem. Chem. Phys.* **2010**, *12*, 4759.
- (30) Berendsen, H. J. C.; v. d. S., D.; van Drunen, R. *Comput. Phys. Commun.* **1995**, *91*, 43.
- (31) Lindahl, E.; Hess, B.; van der Spoel, D. *J. Mol. Model.* **2001**, *7*, 306.
- (32) Hess, B.; Kutzner, C.; van der Spoel, D.; Lindahl, E. *J. Chem. Theory Comput.* **2008**, *4*, 435–447.
- (33) Bussi, G.; Donadio, D.; Parinello, M. *J. Chem. Phys.* **2007**, *126*, 014101.
- (34) Jorgensen, W. L.; Severance, D. L. *J. Am. Chem. Soc.* **1990**, *112*, 4768.

- (35) Synecek, V.; Chessin, H.; Simerska, M. *Acta Crystallogr.* **1970**, *A* **26**, 108.
- (36) McNellis, E. R.; Meyer, J.; Reuter, K. *Phys. Rev. B* **2009**, *80*, 205414.
- (37) Tkatchenko, A.; Scheffler, M. *Phys. Rev. Lett.* **2009**, *102*, 073005.
- (38) Syomin, D.; Kim, J.; Koel, B. E.; Ellison, G. B. *J. Phys. Chem. B* **2001**, *105*, 8387.
- (39) Schravendijk, P.; van der Vegt, N. F. A.; Delle Site, L.; Kremer, K. *Chem. Phys. Chem.* **2005**, *6*, 1866.
- (40) Bilic, A.; Reimers, J. R.; Hush, N. S.; Hoft, R. C.; Ford, M. J. *J. Chem. Theory Comput.* **2006**, *2*, 1093.
- (41) Rappe, A. K.; Casewit, C. J.; Colwell, K. S.; Goddard, W. A., III; Skiff, W. M. *J. Am. Chem. Soc.* **1992**, *114*, 10024.
- (42) Williams, G.; Watts, D. C. *Trans. Faraday Soc.* **1970**, *66*, 80.